Laboratory demonstration of Phase Induced Amplitude Apodization (PIAA) coronagraph with better than 10^{-9} contrast

Brian Kern*[a], Olivier Guyon[b], Andreas Kuhnert[a], Albert Niessner[a], Frantz Martinache[b], Kunjithapatham Balasubramanian[a]
[a]Jet Propulsion Laboratory, California Institute of Technology,
4800 Oak Grove Dr., Pasadena, CA, USA 91109;
[b]The University of Arizona, Steward Observatory, Tucson, AZ USA 85721

ABSTRACT

We present coronagraphic images from the Phase Induced Amplitude Apodization (PIAA) coronagraph on NASA's High Contrast Imaging Testbed (HCIT) at the Jet Propulsion Lab, showing contrasts of 5×10^{-10} averaged from 2-4 λ/D, in monochromatic light at 808 nm. In parallel with the coronagraph and its deformable mirror and coronagraphic wavefront control, we also demonstrate a low-order wavefront control system, giving 100× rms suppression of introduced tip/tilt disturbances down to residual levels of 10^{-3} λ/D. Current limitations, as well as broadband (10% fractional bandpass) preliminary results are discussed.

Keywords: coronagraph, wavefront control

1. INTRODUCTION

1.1 PIAA coronagraph principle

NASA's Jet Propulsion Laboratory (JPL) has a dedicated coronagraphic technology development facility, the High Contrast Imaging Testbed (HCIT). A Phase Induced Amplitude Apodization (PIAA) coronagraph is under test at JPL's HCIT, the results of which are presented in this paper. PIAA is a high-throughput, small inner-working angle, high spatial resolution coronagraphic technique proposed for space-based exoplanet imaging and spectroscopy missions[1-5]. To produce a stellar point-spread function (PSF) with a usable dark hole region with intensity at the 10^{-9} level, a deformable mirror (DM) is used to control the wavefront in the presence of diffraction and optical aberrations.

1.2 PIAA implementation on HCIT

The PIAA mirrors in this report were fabricated by Axsys, and are duplicates ("mirror images") of those described in Ref. 6. They are referred to here as PIAA-1, referencing the first generation of PIAA mirror designs. These are distinct from a second-generation set of PIAA mirrors fabricated by Tinsley, used previously on HCIT[7] and at NASA Ames[8] although they operate on the same PIAA principle. The second-generation mirrors are referred to here as PIAA-2.

The PIAA experiment at HCIT is laid out on a 5'×8' table, in a vacuum chamber. The coronagraph uses several off-axis parabolas (OAPs) as relay optics. The PIAA M2 is conjugated to a postapodizer, which for this experiment is a simple circular stop (a traditional aperture), not an annular binary postapodizer that is typically specified for PIAA coronagraphs, as described and justified in Ref. 9. The postapodizer is then conjugated to the DM. The illumination of the DM covers approximately a 29-actuator diameter circle (out of 32×32 actuators). The light is brought to a focus where an occulter is located, then recollimated to pass through a Lyot stop, and imaged onto a CCD camera. A sketch of the layout is shown in Figs. 1 and 2. Not shown on the figure is a linear polarizer, which is inserted immediately before the science camera. This is discussed in Section 2.2 below.

The PIAA coronagraph also has an integrated Coronagraphic Low-Order Wavefront Sensor (CLOWFS) and associated tip-tilt actuators. Light reflected from the occulter is reimaged (magnified and slightly out-of-focus) on the CLOWFS camera, shown in Fig. 2. The occulter used for this purpose has a central absorbing spot, is reflective on the rest of the substrate, and has a void that transmits light through to the rest of the optical train, shown in Fig. 3. The occulter is

*Brian.D.Kern@jpl.nasa.gov; phone 1 818 395-6024; jpl.nasa.gov

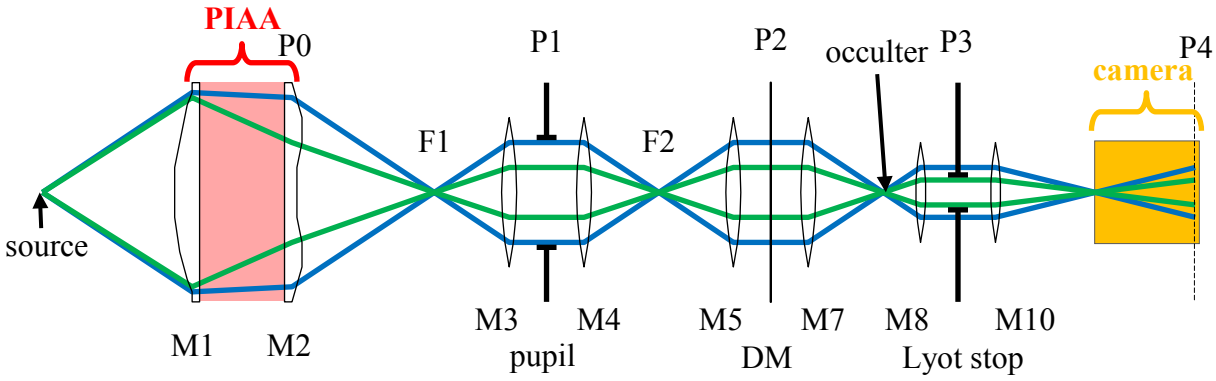

Fig. 1. Unfolded optical train to the science camera, not to scale. The marginal rays defined by the pupil stop (P1) are shown in blue, the marginal rays defined by the Lyot stop (P3) are shown in green. The planes conjugate to the source are easily identified as the locations where marginal rays cross; the occulter lies in a plane conjugate to the source. The planes conjugate to the pupil stop (P1) are labeled P0 – P4, and include PIAA M2 (P0), the DM (P2), and the Lyot stop (P3). The science camera is mounted on a translation stage that can reach a plane conjugate to the source (F4) and, by translating downstream, a plane conjugate to the pupil (P4), a range shown here in orange. The source and occulter can each be moved in 3 dimensions, and the pupil stop and Lyot stop can be removed. The CLOWFS system is not shown in this figure.

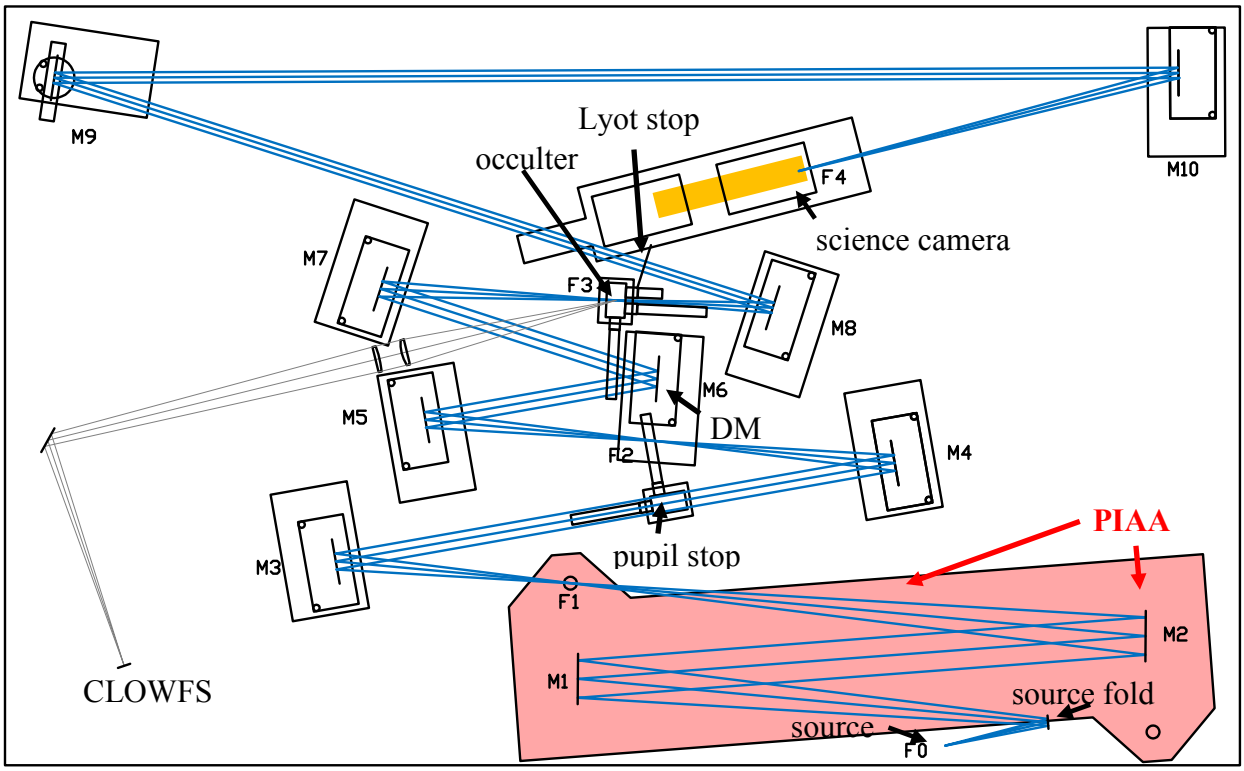

Fig. 2. Layout of optics on table, to scale. The source is at the bottom-right (F0). Light reflected off the occulter (gray rays) is relayed to the CLOWFS camera (bottom left). M9 is a flat mirror. The source fold mirror and DM have piezo actuators for tip-tilt (used by CLOWFS).

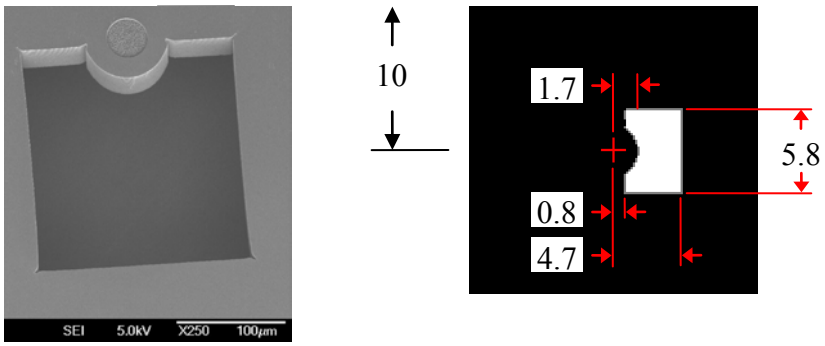

Fig. 3. (LEFT) SEM image of occulter, (RIGHT) measured cculter transmission. This transmission is measured at the science camera, ranging from 0 to 1, seen with the Lyot stop removed. The occulter is positioned so that the source image is centered on the red cross at the center of this image. The full image is ±10 λ/D_{sky} on each side. The inner radius is 1.7 λ/D_{sky}, while the farthest corners are located at 5.5 λ/D_{sky}. The SEM image is of a similar but not identical occulter to the transmission image. The transmission image is the occulter used for the demonstrations in this paper..

freestanding, in the sense that there is no substrate in locations where the transmission is nonzero. The reflected light feeds the CLOWFS system.

The transmission for off-axis sources (i.e., planets) to the science camera is shown in Fig. 4, with three different normalizations. Other coronagraphic testbed demonstrations have normalized transmissions to their own peaks; this is shown in Fig. 4a. Normalizing to the occulter-out, Lyot-in on-axis source image peak leads to Fig. 4b, and normalizing to the occulter-out, Lyot-out on-axis source image peak is shown in Fig. 4c. Fig. 4c shows the full coronagraphic throughput for these off-axis locations. These plots are all for a single polarization component, appropriate to all these demonstrations. With a polarizer in, the transmission for unpolarized light would be half as large.

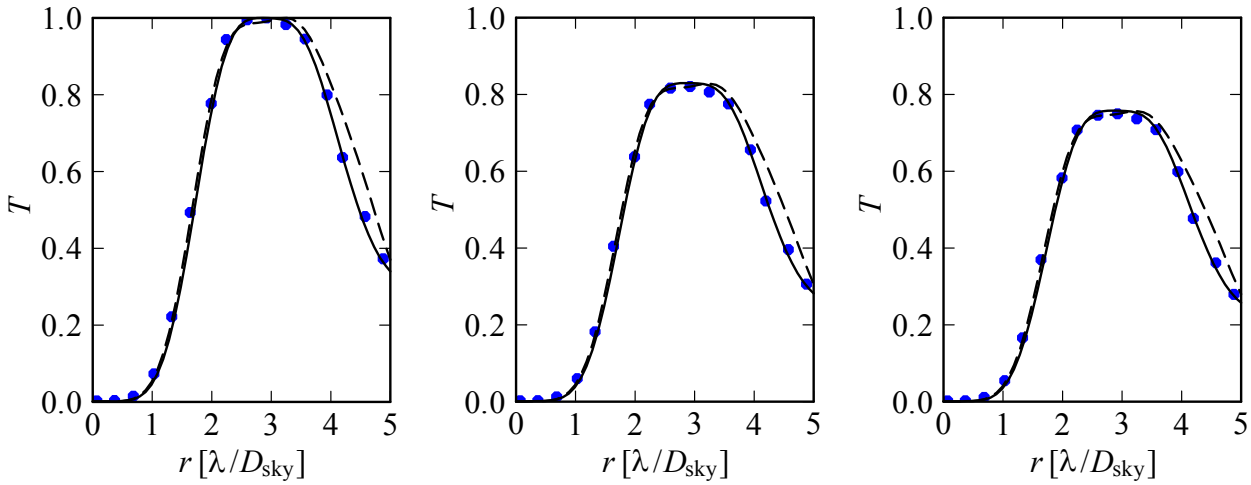

Fig. 4a-c. Coronagraph throughput for off-axis source, with three different normalizations: (a, LEFT) normalized to peak throughput, (b, CENTER) normalized to unocculted, Lyot-in transmission, (c, RIGHT) normalized to unocculted, no-Lyot transmission. In each panel, the solid black line is a model cut along the x axis, the dashed black line is a model cut along a line to the corner of the mask open area, and the blue points are measured along x. The throughput crosses $T = 0.5$ at 1.70, 1.82, and 1.88 λ/D_{sky}.

2. MONOCHROMATIC CONTRAST

2.1 Milestone description

As a part of the NASA TDEM award that funded the PIAA operations at HCIT, a milestone description was negotiated with NASA that specified a 10^{-9} monochromatic demonstration, averaged over a 2-4 λ/D region. This experiment was carried out several times, with somewhat different wavefront control inputs, and somewhat different end results. Images from three different wavefront control runs are shown in Fig. 5. Radial plots of the measured intensities are shown in Fig. 6. The demonstration was carried out using an 808 nm laser source. The result, after wavefront control, was an average intensity of 5×10^{-10}, in the best-case outcome.

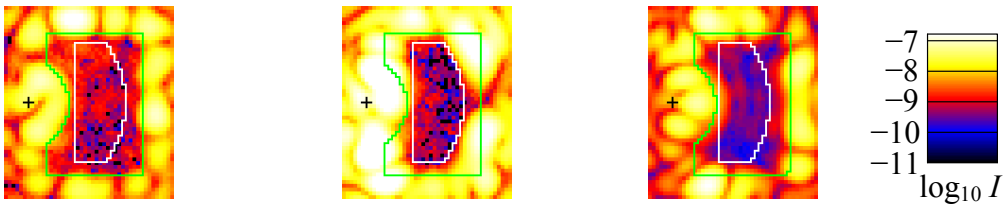

Fig. 5. Monochromatic dark holes, for three different wavefront control runs. The black cross marks the centroid of the unocculted source. The green box shows the transmitting region of the occulter, the white line marks the edge of the "dark hole" where the intensities are measured and averaged. Each image extends from −1 to +6 λ/D in x, +/− 4 λ/D in y.

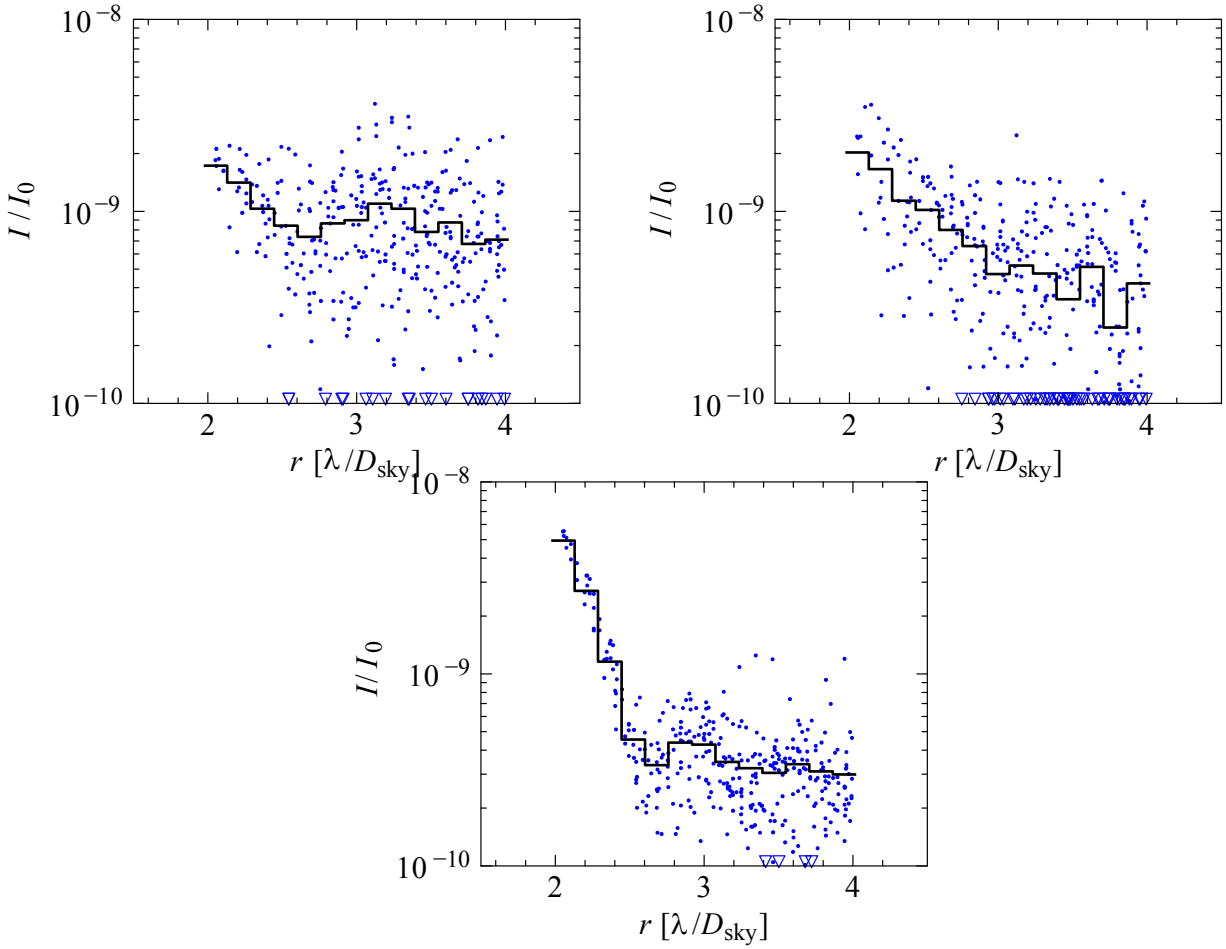

Fig. 6. Radial plots of intensities from Fig. 5. Solid lines are binned by 1 pixel in radius, corresponding to (λ/D_{sky}) / 6.34. Blue points are individual pixel intensity values. Triangles denote points that lie below the bottom edge of the plot.

2.2 Discussion of results

A number of intermediate configurations were tested before arriving at the configuration that delivered < 10^{-9} intensities. The changes from one configuration to the next, which provided some improvement, include changing from a bare fiber illumination at the source to a pinhole, changing the occulter from a pattern-on-glass to freestanding design, the move from in-air testing to testing under vacuum, and the addition of a linear polarizer to the optical train. The mechanism that produces polarization-specific contrast change, and therefore requires a linear polarizer in the system to obtain good contrasts, has not been identified. Calculations of Fresnel reflection coefficients and their effect on polarization states do not predict the size of the effect seen (~ 10^{-8}).

The milestone #1 results have not yet been reviewed by NASA for official acceptance.

3. LOW-ORDER WAVEFRONT CONTROL

3.1 CLOWFS operation

A milestone definition was negotiated for the CLOWFS system as well, which specified a demonstration of 0.01 λ/D rms tip-tilt residuals after correction, and 0.001 λ/D rms calibration accuracy. This milestone was completed and approved by NASA in 2012. The milestone report is available as Ref. 10. The specific details of calibration and algorithm are presented there, and will not be repeated here in as much detail.

The CLOWFS system uses light reflected off the occulter, and a combination of piezo tip-tilt actuators to implement pointing control. There are tip-tilt actuators on the DM mount, and on the fold mirror between the source and PIAA M1, shown in Fig. 2. The camera used was limited by overheating in vacuum, and could operate only with a duty cycle of about 1/5. The operational mode chosen was to operate for 1.2 s out of every 7 s, effectively operating only at 1/7 Hz. At the time of the demonstration, an upgraded camera was on order, expected to operate at approximately 100 Hz. This camera has since arrived, but its performance has not been analyzed in the same way as the data from the milestone demonstration, so the data shown here are from the old, slower camera.

The control loop was constructed as a simple integrator; the residual tip/tilt is measured, and the new correction is applied to the actuators. The limiting timescale in this was the camera power-cycling; images were accumulated for 1.2 s and averaged, the correction is calculated and applied in a small fraction of a second, then nothing happens for the remainder of the 7 s before the next camera image sequence. The corrections were applied with an open-loop gain of unity, i.e., the "entire" correction is applied after every measurement.

Under vacuum, the levels of tip-tilt disturbances were well below the milestone requirements. The in-air disturbance spectrum was applied deliberately to the actuators, at a reduced frequency where the slow camera could operate. The reduction in temporal frequencies at this stage was less than the improvement in temporal frequencies allowed by the newer camera. In principle, this would allow the new camera, operating at higher frequencies, to correct the in-air disturbances to the same levels as this demonstration in vacuum. This has not been tested. However, since the disturbances were input directly, the same exact disturbance time-series could be repeated at different times; therefore, an uncorrected power spectrum could be measured, followed by a closed-loop residual power spectrum, allowing the suppression to be directly measured. This is shown in Fig. 7.

3.2 CLOWFS discussion

The closed-loop rms residuals were near 0.001 λ/D. sufficiently low to ensure negligible dark hole contrast degradation at the 10^{-9} level. However, the temporal frequencies and power spectral shape were not appropriate to a flight environment, nor were the flux rates. This demonstration serves as a confirmation that systematic errors do not prevent operation at 0.001 λ/D levels, and that the power suppression observed at these levels matched predictions. Anywhere that linear models apply, the suppression factors shown here, given enough photons to make adequate measurements, should apply.

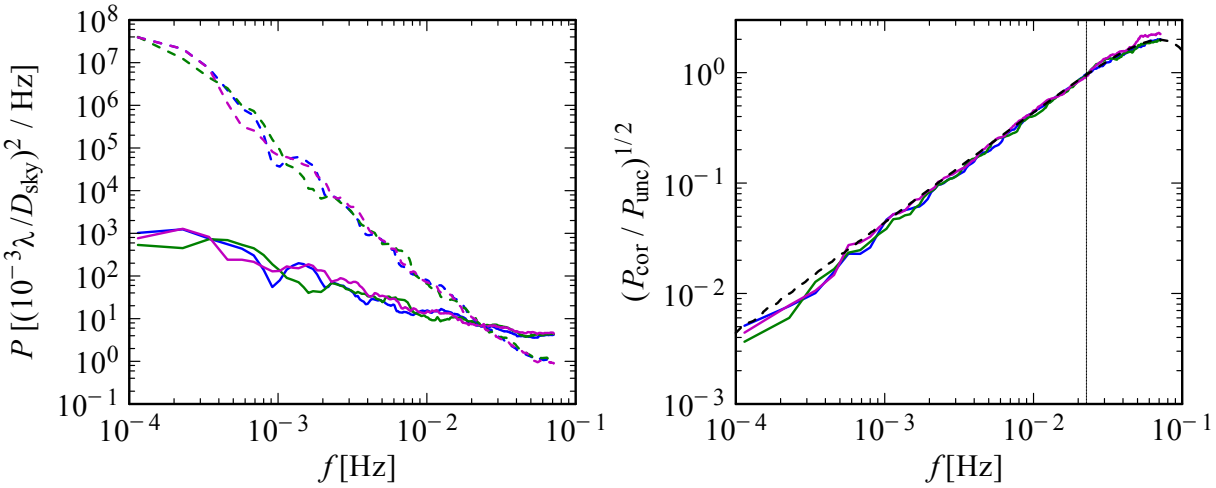

Fig. 7. (LEFT) Tip-tilt power spectra with no correction (dotted line) and closed-loop residuals (solid lines), and (RIGHT) closed-loop gain (suppression ratio), with dotted line for expected gain. In both plots, the three colors denote three separate runs with different input disturbances.

4. BROADBAND (10%) CONTRAST

4.1 Current status

The experimental arrangement inside the vacuum chamber (i.e., all components in Figs. 1 and 2) have been unchanged from the monochromatic to the first broadband experiments. The source, which is fed via single-mode fiber from outside the vacuum chamber onto the table inside, can be exchanged with no in-vacuum changes. A supercontinuum laser source with a series of four contiguous 2.5% bandpass filters was used instead of the 808 nm laser from the monochromatic demonstration. Taken together, these individual filters add to create a 10% bandpass centered at 800 nm. Wavefront estimates at each of the four 2.5% filters were acquired, and fed into a broadband wavefront control algorithm (essentially similar to that in Ref. 11). The results are shown in Figs. 8 and 9, evaluated in the same way as the monochromatic results. The mean intensity in the dark hole, from 2-4 λ/D, was 2.10×10^{-8}. The linear polarizer, described in Sections 1.2 and 2.2, was in place for these observations as well.

4.2 Future direction

Simulations of the expected wavefront control limits, given the initial wavefront produced by the system, show limits for a 7.5% bandpass near the 10^{-8} level, using the PIAA-1 mirrors[12]. The observed 2×10^{-8} levels for a 10% bandpass do not leave much room for improvement down to the predicted levels, with the current hardware. The PIAA-2 mirrors, fabricated at Tinsley, were specified with much smaller tolerances for surface errors. According to the simulations in Ref. 12, reducing the phase and amplitude errors is the key to better broadband performance, interpreted liberally (without having done simulations with the PIAA-2 mirrors specifically). The next step in improving broadband performance will be to exchange the PIAA-1 mirrors for PIAA-2 mirrors.

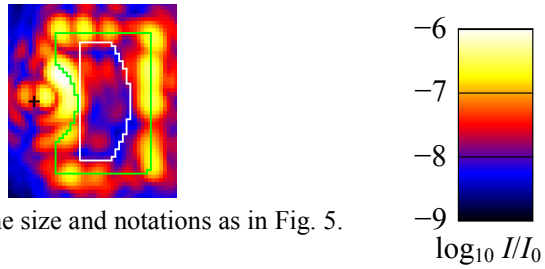

Fig. 8. Dark hole with 10% broadband light. Same size and notations as in Fig. 5.

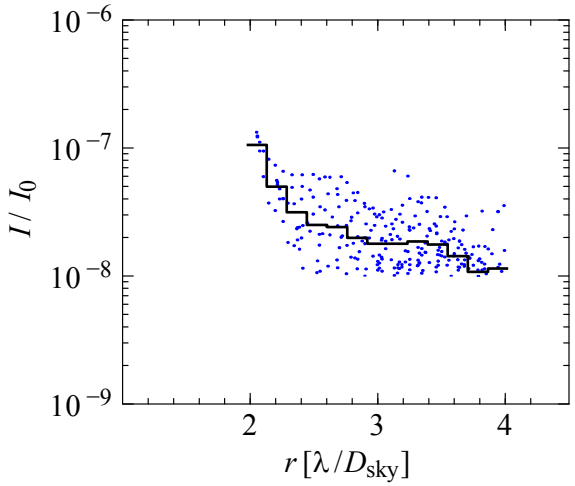

Fig. 9. Radial plot of 10% broadband dark hole intensity, same notation as Fig. 6.

5. CONCLUSIONS

The PIAA laboratory demonstrations described here show performance at levels relevant to space mission requirements. These are among the highest contrast results demonstrated to date, and are compared to other coronagraph architectures in Ref. 13. The path toward higher contrast or higher bandwidth is likely to require smaller surface errors than those present on the PIAA-1 mirrors, which will be replaced at HCIT soon with PIAA-2 mirrors (with smaller surface errors). The sensitivity to polarization remains a mystery, and will be investigated after wavefront control and bandwidth demonstrations have completed.

ACKNOWLEDGEMENTS

This research was carried out at the Jet Propulsion Laboratory, California Institute of Technology, under a contract with the National Aeronautics and Space Administration.

REFERENCES

[1] Guyon, O. et al., "The pupil mapping exoplanet coronagraphic observer (PECO)," Proc. SPIE 7731, 773129 (2010).
[2] Trauger, J. et al., "ACCESS: a concept study for the direct imaging and spectroscopy of exoplanetary systems," Proc. SPIE 7731, 773128 (2010).
[3] Guyon, O. et al., "Exoplanet imaging with a phase-induced amplitude apodization coronagraph. I. Principle," Astrophys. J. 622, 744-758 (2005).
[4] Vanderbei, R.J., Traub, W.A., "Pupil mapping in two dimensions for high-contrast imaging," Astrophys. J. 626, 1079-1090 (2005).
[5] Guyon, O. et al., "Theoretical limits on extrasolar terrestrial planet detection with coronagraphs," Astrophys. J. Supp. Series 167, 81-99 (2006).
[6] Guyon, O et al., "High-Contrast Imaging and Wavefront Control with a PIAA Coronagraph: Laboratory System Validation," Pub. Astron. Soc. Pacific 122, 71-84 (2010).
[7] Kern, B. et al., "Phase-induced amplitude apodization (PIAA) coronagraph testing at the High Contrast Imaging Testbed," Proc. SPIE 7440, 74400H (2009).
[8] Belikov, R. et al., "EXCEDE technology development I: first demonstrations of high contrast at 1.2 lambda/D for an Explorer space telescope mission," Proc. SPIE 8442, 844209 (2012).

[9] Kern, B. et al., "Laboratory testing of a Phase-Induced Amplitude Apodization (PIAA) coronagraph," Proc. SPIE 8151, 815104 (2011).
[10] Guyon, O., Kern, B., Martinache, F., "Phase-Induced Amplitude Apodization (PIAA) Technology Development, Milestone #2; Instrument Tip-Tilt Control Demonstration at Sub Milliarcsecond Levels," http://exep.jpl.nasa.gov/files/exep/PIAAmilestone2_final120821.pdf (2012).
[11] Give'on, A., Kern, B., Shaklan, S., Moody, D.C., Pueyo, L., "Broadband wavefront correction algorithm for high-contrast imaging systems," Proc. SPIE 6691, 66910A (2007).
[12] Sidick, E. et al., "Comparison of Simulated Contrast Performance of Different Phase Induced Amplitude Apodization (PIAA) Coronagraph Configurations," Proc. SPIE 8864, this conference (2013).
[13] Lawson, P. et al., "Survey of experimental results in high-contrast imaging for future exoplanet missions," Proc. SPIE 8864, this conference (2013).